Nano Energy 139 (2025) 110950

Contents lists available at ScienceDirect

Nano Energy

journal homepage: www.elsevier.com/locate/nanoen

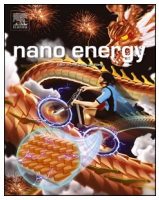

Mitigating electrode polarization through electrolyte concentration optimization

Weibin Chen [a,b,1], Kai Wang [c,1], Xuanlong He [a], Xi Chen [a], Tao Huang [a], Jing Chen [d], Weiyuan Huang [c], Xuming Yang [a,b], Xiangzhong Ren [a], Xiaoping Ouyang [a,d], Jianhong Liu [a,b], Feng Pan [c,*], Biwei Xiao [e,*], Qianling Zhang [a,b,**], Jiangtao Hu [a,b,**]

[a] Graphene Composite Research Center, College of Chemistry and Environmental Engineering, Shenzhen University, Shenzhen 518060, PR China
[b] Shenzhen Key Laboratory of Functional Polymers, College of Chemistry and Environmental Engineering, Shenzhen University, Shenzhen 518060, PR China
[c] School of Advanced Materials Shenzhen Graduate School, Peking University, Shenzhen 518060, PR China
[d] School of Materials Science and Engineering, Xiangtan University, Xiangtan 411105, PR China
[e] GRINM (Guangdong) Research Institute for Advanced Materials and Technology, Foshan, Guangdong 528051, PR China

ARTICLE INFO

Keywords:
High-loading electrode
Electrolyte concentration optimization
Mitigating electrode polarization
Percolation network optimization

ABSTRACT

High-loading electrodes are crucial for attaining elevated high energy density in the industrial applications of lithium-ion batteries. However, a rise in electrode loading correlates with an elevation in electrode tortuosity. The elevated tortuosity of the transport pathway may result in a discrepancy between ion transport and electrode reaction, leading to excessive or incomplete reactions of localized particles, creating concentration gradient phenomena, and ultimately causing capacity loss. Research on high-loading electrodes mostly concentrates on the regulation of electrode structure and material modification, while investigations into electrolyte concentration predominantly emphasize solvation structures; however, the correlation between electrolyte concentration and high-loading electrodes has been inadequately explored. This study examines the effect of electrolyte concentration on the electrochemical performance of high-loading $LiNi_{0.83}Mn_{0.12}Co_{0.05}O_2$ (NMC83) electrode. Utilizing pore network modeling (PNM), high-resolution techniques, and pore equivalent diameters (EqD) analysis to compare ion transport pathways and abilities under different electrolyte concentrations. It was observed that a concentration of 1.5 M in the conventional electrolyte can establish a more efficient percolation channel and provide sufficient lithium ions to achieve a balance between ion transport and electrode reaction, thereby alleviating the inherent concentration polarization of high-loading electrodes.

1. Introduction

With the swift development of new energy, the emerging opportunities in the electric vehicle (EV) market and grid-scale storage call for lithium-ion batteries (LIBs) with a higher energy density (>500 Wh kg^{-1} at the cell level) and a lower price (< \$100 $(kWh)^{-1}$ at the pack level) [1]. High-loading electrode design is extensively utilized to optimize specific energy and minimize the total package cost in the pursuit of high-performance battery systems.[2] Nevertheless, increasing electrode loading results in elevated battery polarization and a decrease in battery power density, constituting a significant technical bottleneck in the industry.[3]

Material modification and electrode structure optimization are the most commonly employed techniques for addressing high-loading electrode issues.[4–10] The core principle of the aforementioned technique is to achieve rapid lithium-ion transfer, both within the material and across the electrode. Material optimization can enhance the intrinsic conductivity of the electrode, a goal likewise sought by material synthesizers. For instance, Pan *et al.*[11], utilizing first-principles calculations in combination with percolation theory and Monte Carlo simulations, have revealed the crucial role of lithium content in inhibiting oxygen loss in lithium-rich cathode materials, establishing a

* Corresponding authors.
** Corresponding authors at: Graphene Composite Research Center, College of Chemistry and Environmental Engineering, Shenzhen University, Shenzhen 518060, PR China.
E-mail addresses: panfeng@pkusz.edu.cn (F. Pan), xiaobiwei@grinm.com (B. Xiao), zhql@szu.edu.cn (Q. Zhang), hujt@szu.edu.cn (J. Hu).
[1] Weibin Chen and Kai Wang contributed equally to this work.

https://doi.org/10.1016/j.nanoen.2025.110950
Received 18 February 2025; Received in revised form 16 March 2025; Accepted 31 March 2025
Available online 1 April 2025

relationship between the migration network of oxygen ions and the transition metal (TM) component. The importance of rational compositional design in lithium-rich cathodes lies in effectively suppressing irreversible oxygen release and enhancing solid-phase diffusion within electrodes. For the design of the electrode structure, the diffusion efficiency of the electrolyte within the electrode is primarily achieved through the construction of gradient pores or gradient particle sizes. For instance, Wu *et al.*[12] constructed a low-tortuosity thick electrode by applying an external magnetic field, presenting uniform lithium-ion reaction kinetics within the electrode. Yu *et al.*[13], employed a modified ice-templating method to fabricate low-tortuosity porous electrodes with tunable wall thickness and channel width, achieving smaller ion transport impedance inside the pore space and faster overall ion diffusion kinetics. In our previous work[9], we designed a rapid electrolyte diffusion pathway to diminish lithium concentration polarization for the high-loading NMC83 electrode by employing two layers of NMC83 materials with different particle sizes. So far, the current focus of research at the electrolyte has primarily been on enhancing battery stability, with limited exploration into the optimal concentration of electrolytes at the high-loading electrodes. This is due to a consensus that a 1 M concentration exhibits maximum ionic conductivities and is considered the most favorable choice. Considering the significance of high-loading electrodes in enhancing the energy density of lithium batteries, it is crucial to investigate the optimal electrolyte concentration for high-loading electrodes.[14]

In this work, we provide 3D-visualized insights into the nature of liquid phase ion transport under different electrolyte concentrations. Facilitated by a combination of pore network modeling (PNM), high-resolution techniques, and pore equivalent diameters (EqD) analysis to compare ion transport pathways and abilities under different electrolyte concentrations. Simultaneously, a comprehensive investigation into the underlying machanisms is conducted by analyzing the lithium-ion transfer kinetics using DRT and GITT, as well as the interphase evolution through XPS and TEM. It was found that the conventional concentration electrolyte (1 M) does not provide a sufficient supply of lithium ions to alleviate concentration polarization,[15] and the concentrated electrolyte ($\geq$ 2 M) with overly high viscosity simultaneously affects lithium-ion transport, exacerbating concentration polarization. Furthermore, the percolation channels formed by both aforementioned methods cannot meet the requirements of high-loading batteries. For high-loading electrodes, the highly convoluted transport pathways result in a significant disparity between the sluggish lithium-ion transport and the lithiation/delithiation processes, which in turn leads to localized over/under lithiation and capacity degradation. Nevertheless, a concentration of 1.5 M in the conventional electrolyte can establish a more efficient percolation channel and supply sufficient lithium ions to alleviate the inherent concentration polarization in high-loading electrodes, achieving a balance between ion transport and electrode reaction. Full cells utilizing a 1.5 M conventional electrolyte exhibit superior cycling stability, mataining a capacity retention rate of 92.3 % after 500 cycles, even in condtions of extremely low porosity ($<$ 35 %).

2. Results and discussion

2.1. Prepare electrolytes with different concentrations

Four electrolytes with different concentrations were prepared, including 1 M, 1.5 M, 2 M, and 2.5 M $LiPF_6$ in a mixture of ethylene carbonate (EC) and ethyl methyl carbonate (EMC) at a ratio of 3:7 (m/m), incorporating 1 ωt% vinylene carbonate (VC), which were defined as E1, E1.5, E2, and E2.5. Due to the disadvantages of high-concentration electrolytes (close to a saturated state), such as limited ionic conductivity, elevated cost, and high weight, their application in high-loading electrodes and high-energy density batteries is seldom considered. Despite a 1 M concentration of electrolyte exhibiting the highest ionic conductivity, whether it is the optimal choice for high-loading electrodes remains uncertain. Within the concentration range of 1 M to high concentration (saturated state), the decrease in lithium-ion transfer rate in the electrolyte may not necessarily be solely attributed to the rate-determining step affecting electrochemical performance, as the Li-ion supply capability is enhanced.

The concentration-dependent Raman spectra in the range from 700 to 1000 cm^{-1} exhibit the EC ring breathing modes with and without Li^+ coordination, as well as the $O-CH_3/O-C_2H_5$ stretching modes of EMC with and without Li^+ coordination (Fig. 1**a**). In the presence of a 1 M $LiPF_6$ in an EC/EMC solution, a distinct peak at approximately 888 cm^{-1} is observed for the EC ring breathing mode[16], along with a broad band centered at approximately 926 cm^{-1} corresponding to the $O-CH_3/O-C_2H_5$ stretching mode of EMC. With the increasing concentration of $LiPF_6$, there is a gradual decrease in intensity for the EC ring breathing band (approximately 888 cm^{-1}), which is progressively replaced by another sharp peak at higher wavenumbers (around 900 cm^{-1}). Similarly, the band intensity of $O-CH_3/O-C_2H_5$ stretching in EMC (approximately 926 cm^{-1}) is gradually reduced with the increasing of $LiPF_6$ concentration, which is accompanied by the appearance and growth of another broad band at approximately 937 cm^{-1} . These two new bands centered at approximately 900 and 937 cm^{-1} can be assigned to Li^+-coordinated EC and EMC. Furthermore, the appearance and growth of Li^+-coordinated EC and EMC bands with increasing $LiPF_6$ concentration are accompanied by an increasing intensity of a new band centered at approximately 736 cm^{-1} , which can be attributed to the $P-F$ symmetric stretching vibration of PF_6^-.[17] At $LiPF_6$ concentrations over 1.5 M, a peak shoulder emerges on the high wavenumber side, indicating the formation of complexes between Li^+ ions and PF_6^- anions or contact ion pairs (CIP). As the concentration of $LiPF_6$ increases, the interionic distance in solution decreases, facilitating ion-pair formation and aggregation (Fig. 1**b**). Moreover, it is evident that an elevation in electrolyte salt concentration results in heightened viscosity and a simultaneous decrease in ionic conductivity (Figs. 1**c** and 1**d**), aligning with previous findings.[18,19]

2.2. Electrochemical performance

Electrode calendaring is a crucial pre-processing step for thick electrode application as it not only enhances the volumetric energy density of electrode materials but also mitigates the impact of electronic conductivity on the rate/cycling performance of high-loading electrodes by reducing the electronic transport distance. Consequently, minimizing the unoccupied space within the electrode is desirable. However, excessive calendaring can impede Li^+ diffusion and diminish the capacity of the electrode material. The cycle performance of Graphite (4.28 mAh cm^{-2})||NMC83 (3.82 mAh cm^{-2}) full cells and the rate performances of Li||NMC83 half cells were evaluated at room temperature in different electrolytes (E1, E1.5, E2, and E2.5) and porosities (55 %, 45 %, 35 %, and 25 %). Fig. S1 demonstrates that as the electrolyte concentration increases, the rate performance declines for varying porosities (55 %, 35 %, and 25 %). For porosities of 55 % and 35 %, the capacity disparity between E1 and E1.5 is less than 10 mAh g^{-1} at current densities of 0.5 C and 1 C (where 1 C = 210 mA g^{-1}). However, the rate performance significantly deteriorates for E2 and E2.5 due to an increase in viscocity and a decrease in conductivity, which hinders the rapid migration of Li^+ in the electrolyte, exacerbating concentration polarization.

The cycle stabilities of Graphite||NMC83 full cells present different phenomena compared to the rate performance. As shown in Fig. 2**a-d,** the cycle performance of the E1.5 electrode is significantly better than that of E1, E2, and E2.5. Specifically, for different porosities (55 %, 45 %, 35 %, and 25 %), E1.5 presents capacity retentions of 92.3 %, 94.1 %, 98.2 %, and 96.8 % for 200 cycles, respectively (Fig. 2**e**). In Fig. 2**e**, it is observed that the capacity retention rates in E2 and E2.5 after 200 cycles are higher than 100 %. This can be attributed to the

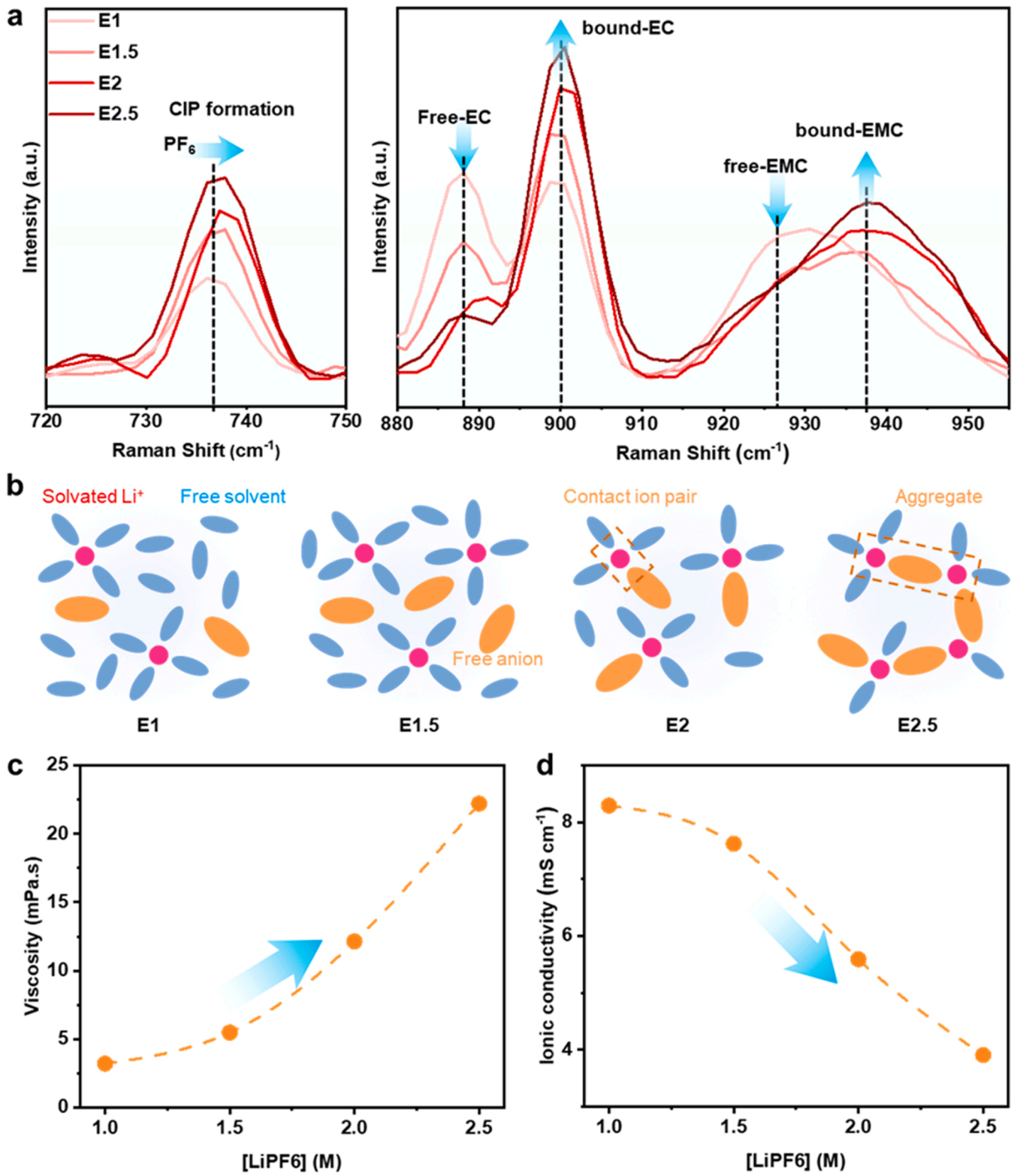

Fig. 1. Characterizations of different concentration electrolytes. Raman spectra (a) and solvation structure (b) in different electrolytes (E1, E1.5, E2, and E2.5). Viscosity (c) and ionic conductivity (d) of different electrolytes (E1, E1.5, E2, and E2.5).

excessive salt concentration and low porosity; the electrolyte infiltration is insufficient, which affects the capacity presentation. However, as the cycle progresses, the electrolyte gradually infiltrates inside the electrode, resulting in a higher capacity retention rate after 200 cycles.[20] Nevertheless, the discharge capacities are lower compared to the cells tested in E1 and E1.5. As shown in Fig. S2a-**d**, the charge/discharge curves of individual electrodes using different electrolytes were evaluated in Graphite||NMC83 full cells. E1.5 enables the NMC cathodes to exhibit much higher accessible charge and discharge capacities, as well as lower polarizations compared to E1, E2, and E2.5. A further comparison of the 500-cycle performance of E1.5 under different electrode porosities is presented in Fig. 2**f**. After 500 cycles, a capacity retention

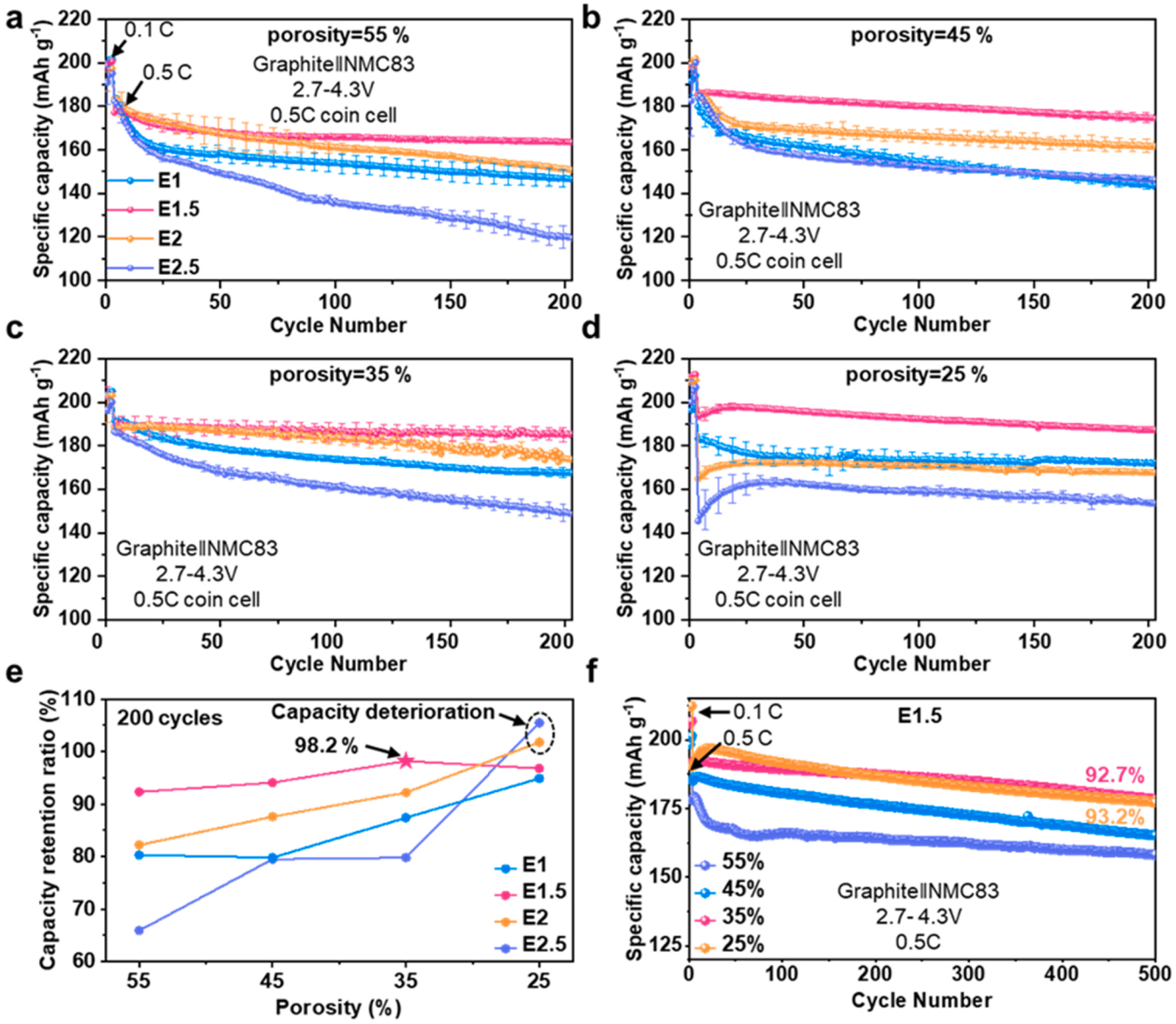

Fig. 2. Electrochemical performances of Graphite‖NMC83 coin cells tested in different electrolytes. (a-d) Cycling performances of Graphite‖NMC83 full cells for 200 cycles using different electrolytes at different cathode porosities, including 55 % (a), 45 % (b), 35 % (c), and 25 % (d) with error bars displayed in insets. The corresponding testing temperature and current density are 25 °C and 0.5 C. (e) The Capacity retention ratios were obtained from the data presented in (a-d). (f) The Cycling performances of Graphite‖NMC83 full cells for 500 cycles with different electrode porosities (55 %, 45 %, 35 %, and 25 %) in E1.5 electrolyte.

rate of 92.7 % was observed at a porosity of 35 %, and stable cycling was also achievable with an ultra-low porosity level of 25 %.

2.3. *Analysis of Li-ion transfer kinetics and characterization of interfacial evolution*

Zhang *et al.* acquired the impedance spectra of the anode and cathode in standard electrolytes via dynamic electrochemical impedance spectroscopy (DEIS). They analyzed the ohmic resistance (R_s) of the bulk electrolyte, the contact resistance (R_{con}) among electrode particles, and the charge transfer resistance (R_{CT}). The impedance on the cathode side surpassed that on the anode side, signifying that the cathode side dictates the rate. Consequently, this research concentrates on the cathode side.[21] To evaluate the kinetic evolution of the Li^+ interfacial transfer process in the NMC83 cathode, concentration-dependent electrochemical impedance spectroscopy (EIS) was employed in Li‖NMC83 half cells.[22] The presence of a semicircular overlap in Nyquist plots often obscures accurate differentiation between the resistance evolution of individual processes due to their similar relaxation time constant (τ).[23–25] To address this issue, the distribution of relaxation time (DRT) technique was utilized to decouple the intertwined electrochemical processes of interphase Li^+ transport, charge transfer, and Li^+ diffusion. DRT transforms frequency-domain Nyquist plots into time-domain-based spectra without pre-modeling the electrochemical system.[26,27] This enables the accurate identification of specific electrochemical processes with similar time constants through the formation of peaks at specific relaxation times.

Fig. 3**a-d** present DRT profiles converted from Nyquist plots (Fig. S3) of Li‖NMC83 half cells tested in different electrolytes at the 1st and 10th cycles. The peak in the relaxation time range of 10^{-6} to 10^{-5} s corresponds to the process of Li^+ transfer across the cathode electrolyte interphase (CEI) (τ1), while the peak in the range of 10^{-5} to 10^{-1} s represents the charge transfer process (τ2). The peaks in the range of 10^{-1} to 10^{2} s represent the Li^+ diffusion impedance (τ3/τ4).[26,28] Specifically, during the first cycle, an intriguing phenomenon has been observed: the corresponding DRT curves of the four electrolytes exhibit

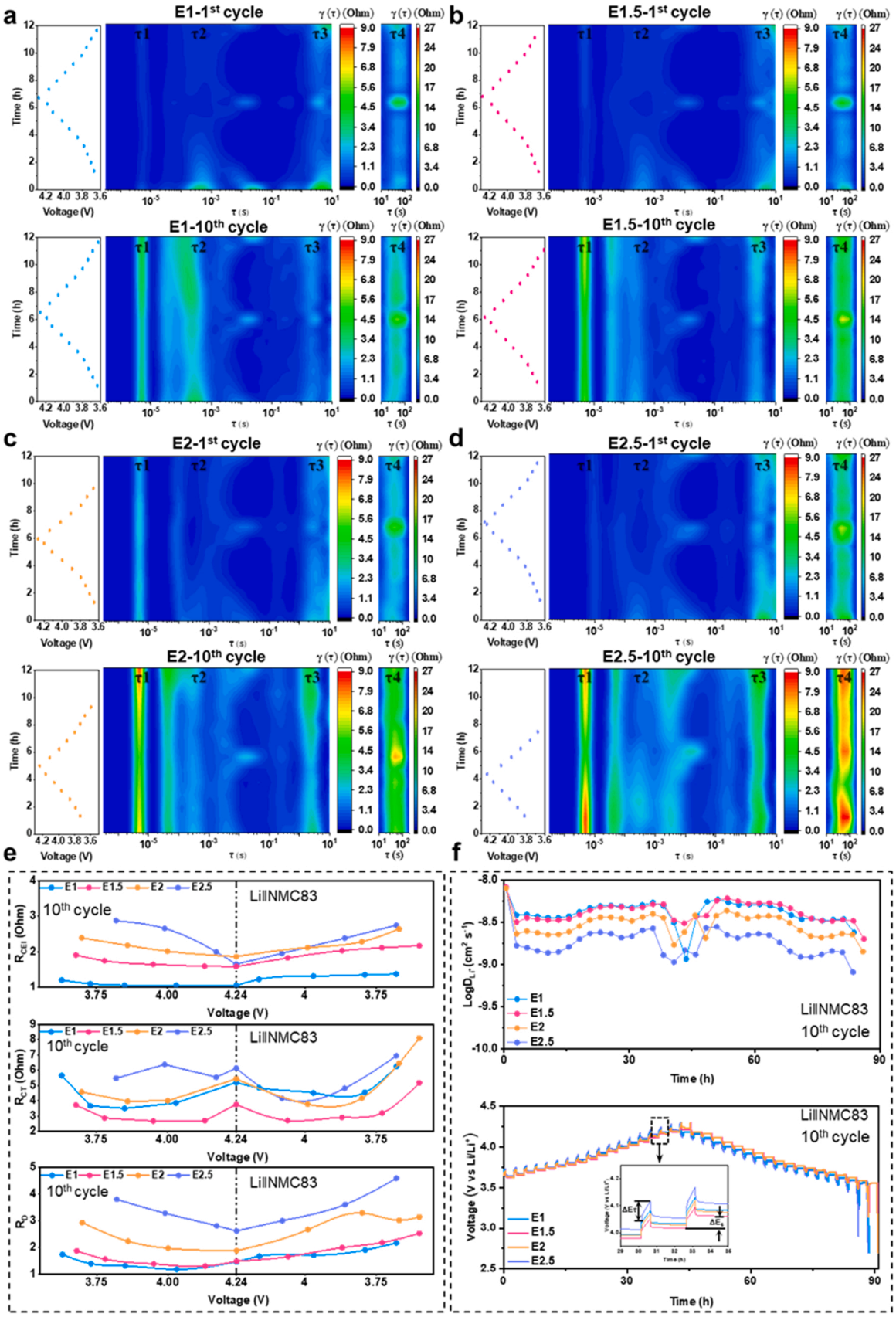

Fig. 3. Analysis of Li^+ transport kinetics of different electrolytes. (a-d) DRT profiles of Li||NMC83 cells at the 1st and 10th cycles in different electrolytes, including E1 (a), E1.5 (b), E2 (c), and E2.5 (d). (e) R_{CEI}, R_{CT}, and R_D of Li||NMC83 cells at the 10th cycle in different electrolytes (E1, E1.5, E2, and E2.5) were calculated by the integration of the corresponding peak area in the DRT profiles. (f) GITT curves and calculated Li^+ diffusion coefficients (D_{Li+}) of Li||NMC83 cells at the 10th cycle.

good symmetry. After 10 cycles, the symmetry of the DRT curves corresponding to E1, E2, and E2.5 deteriorated significantly. However, for E1.5, the DRT curves comprising τ1, τ2, τ3, and τ4 demonstrate excellent symmetry during the first 10 cycles (Fig. 3**a-d**). The DRT symmetry both before and after the cycling suggests that there is no significant depletion of lithium ions or solvent molecules in the electrolyte following charge and discharge processes. This phenomenon can be attributed to the stability of the CEI film, which alleviates the lithium-ion consumption during cycling.

Moreover, the values of resistance of CEI (R_{CEI}), charge transfer (R_{CT}), and Li^+ diffusion impedance (R_D) were determined by integrating the corresponding peak areas; notably, the R_D includes the diffusion impedance of Li^+ in the active substance and electrolyte.[29] As illustrated in Fig. 3**e**, it is evident that the R_{CEI} exhibits a positive correlation with the electrolyte concentration. For R_{CT}, the value of E1.5 is the lowest, indicating superior solvation and desolvation abilities. Regarding R_D, there was little difference between E1 and E1.5, while E2 and E2.5 had significantly deteriorated lithium-ion diffusion impedance. The GITT analysis (Fig. 3**f**) further evaluated the Li^+ diffusion coefficient (D_{Li}^+) across various electrolytes, revealing a consistent trend. We hypothesized that an appropriate increase in electrolyte concentration to 1.5 M facilitates the formation of an effective Li^+ percolation network within the electrode, which can alleviate the imbalance between ions and electrode reactions in high-loading electrodes, eliminate concentration polarization, and thereby compensate for the diminished diffusion capacity of lithium ions due to increased electrolyte viscosity.

To systematically investigate the interfacial evolution of cells with different electrolytes, X-ray photoelectron spectroscopy (XPS) and transmission electron microscopy (TEM) were performed. Pronounced peaks corresponding to abundant LiF were observed at 685.1 eV in the F 1 s spectra for E1.5, whereas these peaks were less prominent in E1, E2, and E2.5 (Fig. 4**a**). The inorganic-rich CEI, particularly the LiF-rich CEI, exhibits a weaker bond to transition metal oxide cathodes, which allows it to experience less strain or stress during the volume change of the cathode, thereby preserving its protective function.[30–32] To gain a more comprehensive understanding of the morphologies of the CEI layers, TEM images of the NMC surfaces at different electrode positions were collected (Fig. 4**b** and **c**). The results indicated that the CEI film on the electrode surface exhibited superior uniformity compared to that observed inside the electrode, particularly for E1, E2, and E2.5. For E1.5, a thin, dense, and uniform CEI film was observed on both the surface and internal positions of the NMC electrode, with a thickness of 1.3 nm and 1.1 nm, respectively. However, the CEI films generated by the other three electrolytes displayed inconsistent thicknesses. The formation of the thin and dense CEI film with E1.5 facilitates the establishment of an effective lithium-ion percolation network within the electrodes, which is conducive to mitigating the inherent concentration polarization associated with thick electrodes. Furthermore, these observations are consistent with the DRT interface dynamics analysis.

2.4. Degree of concentration polarization under different electrolytes

To further elucidate the impact of the Li^+-transport path on electrodes with different electrolytes, the structural changes of the electrodes before and after cycling were measured by X-ray computed tomography (XCT) (Fig. 5a). This technique allows for direct visualization of the 3D structure of the electrode.[5,33–36] The dark grey areas represent regions occupied by NMC particles, carbon black, and binder, while the orange areas represent the pore regions. To quantify the percolation paths, a pore network model (PNM) was constructed based on the XCT results, and the actual geometric characteristics of different pore equivalent diameters (EqD) were measured. As shown in Fig. 5b, based on the principle of the maximal sphere algorithm [37], the pores were approximated as spheres and the pore channels as throats (Fig. S4) to construct the PNM; the intensity bar (from purple to red) represents the transport distance (from short to long) within the connection network. In terms of sparsity, E1.5 and E2.5 establish a denser percolation network than E1, indicating more throats connected to the pores, hence enhancing the connectivity structure and facilitating the formation of more efficient percolation channels.[38] In terms of transmission distance, E1 and E1.5 have a lower red proportion compared to E2.5, indicating shorter percolation pathways. Given the scarcity of PNM and the transmission distance, E1.5 is optimal, whereas E1 and E2.5 are comparatively inferior. Concurrently, the corresponding average throat length and pore form factor were subsequently extracted (Fig. S5a-b). It was observed that E1.5 exhibited the shortest average throat length and the largest pore form factor, followed by E1, with E2.5 being the least favorable. A shorter average throat length implies a shorter fluid passage path through the throat, thereby reducing the experienced frictional and viscous resistance. A larger pore shape factor indicates a more circular pore shape, suggesting a smoother percolation path and lower tortuosity.

Furthermore, the pores within the electrodes were classified into macropores (EqD $\geq$ 40 μm), mesopores (20 μm $<$ EqD $\leq$ 40 μm), micropores (10 μm $<$ EqD $\leq$ 20 μm), and nanopores (EqD $\leq$ 10 μm), and their respective proportions were analyzed (Fig. 5**c** and Fig. S6). The analysis revealed that E1 exhibited a relatively high proportion of macropores, whereas E1.5 demonstrated a more concentrated distribution of mesopores, both configurations conducive to the formation of favorable lithium-ion percolation channels. In contrast, E2.5, due to the uneven CEI film, displayed a higher proportion of micropores and a reduced proportion of macropores and mesopores, resulting in tortuous lithium-ion percolation channels that hindered the transport of lithium ions. Consequently, both E1 and E1.5 are capable of forming rapid lithium-ion percolation networks, while the percolation network of E2.5 is relatively tortuous. The rapid lithium-ion percolation network facilitates the fast and efficient transport of lithium ions, alleviating the inherent concentration polarization of high-loading electrodes, reducing the imbalance between ion transport and electrode reactions, and achieving a reasonable de-lithiation/lithiation of active materials in thick electrodes, thereby enhancing the cycle life and capacity of the battery. [8,39–41]

Generally, an appropriate electrolyte concentration and a uniform CEI film are essential to address the challenges encountered in high-loading electrodes, particularly under conditions of low porosity. For instance, the 1.5 M electrolyte applied in this work provides an adequate supply of lithium ions [42–44], facilitating the formation of a dense and uniform CEI layer. Through the synergistic effect of multiple factors, the inherent concentration gradient phenomenon in thick electrodes is alleviated, achieving a balance between ion transport and electrode reaction. However, the conventional 1 M electrolyte fails to provide sufficient lithium ions, thus being unable to meet the continuous lithium-ion transport demands of high-loading batteries. In the case of concentrated ($\geq$ 2 M) electrolytes, the formation of an uneven CEI film after long-term cycling and the severe deterioration of the CEI film inside the electrode lead to the creation of tortuous percolation pathways and potentially the blockage of these pathways, exacerbating the concentration gradient issue. Neither low nor high concentration electrolytes can alleviate the inherent concentration polarization problem of high-loading electrodes, which can lead to excessive or incomplete reactions among local particles, ultimately resulting in battery failure.[15]

3. Conclusion

In summary, this study provides 3D visualizations that offer deep insights into the mechanisms of liquid-phase ion transport within electrolytes of varying concentrations and explores the optimal electrolyte concentration formulation in high-loading electrodes. The full cells with an electrolyte concentration of 1.5 M in the conventional electrolyte exhibit exceptional cycle performance, achieving a capacity retention rate of 92.3 % even after 500 cycles under extremely low porosities ($<$ 35 %), which is superior to that of the full cells with other electrolyte

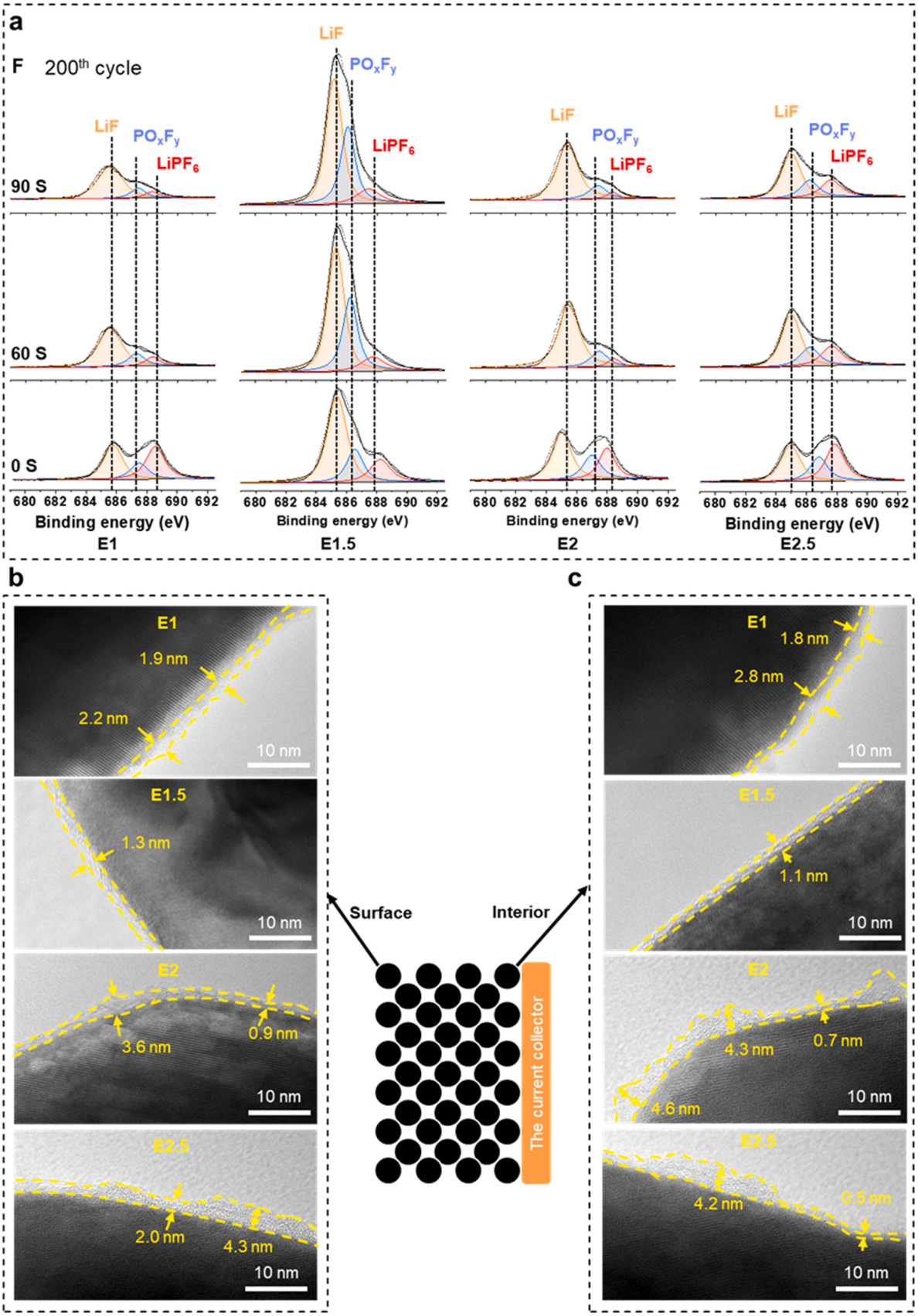

Fig. 4. Interphasial evolution of NMC83 cathodes of different electrolytes. (a) XPS spectra of the CEI on NMC83 cathodes at the 200th cycle in different electrolytes (E1, E1.5, E2, and E2.5) displayed in columns alongside the corresponding depth profiling results. (b and c) TEM images of NMC83 cathode surfaces (b) and interiors (c) in different electrolytes (E1, E1.5, E2, and E2.5) at the 200th cycle.

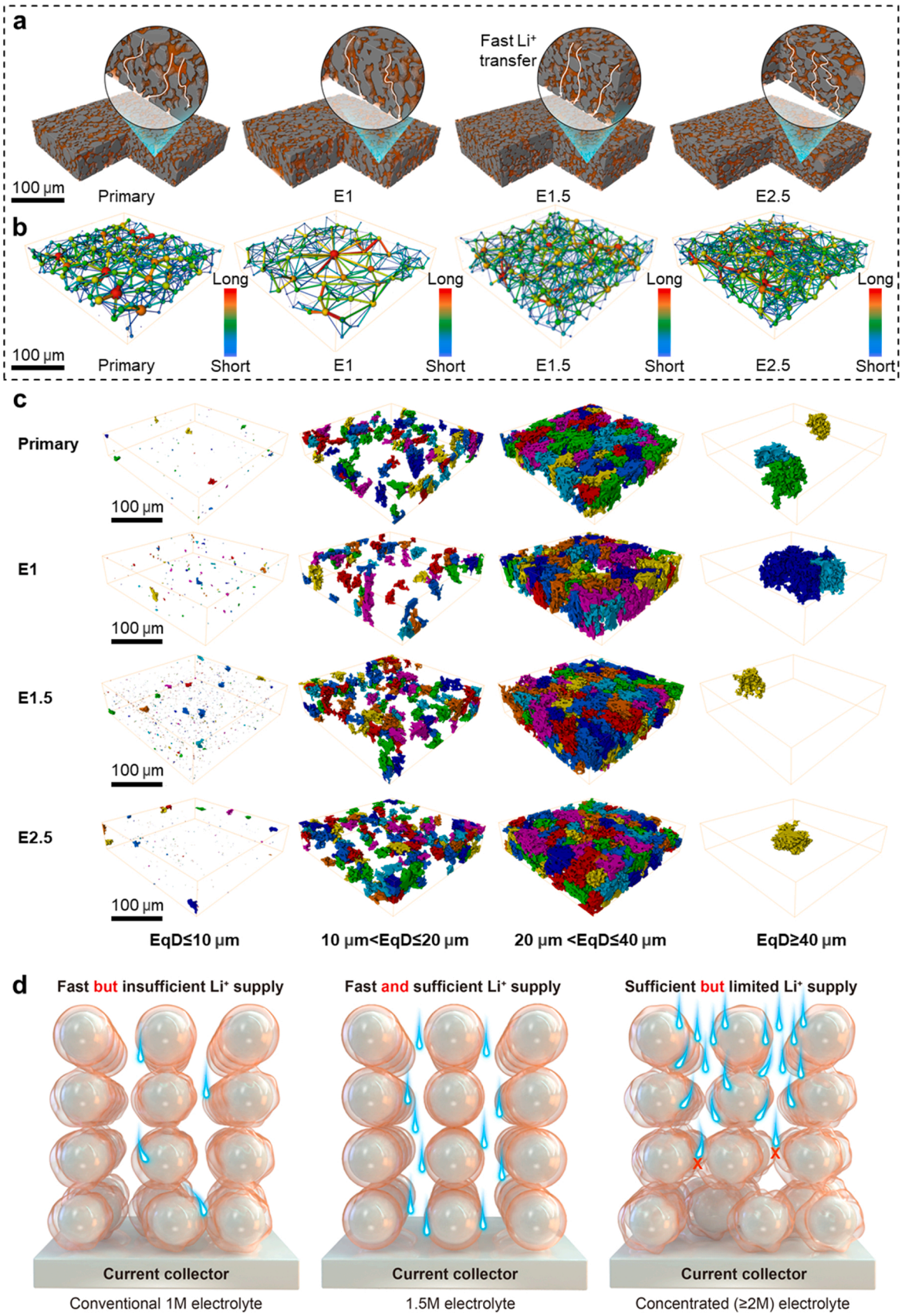

Fig. 5. 3D characterization of the NMC cathode based on the XCT data. (a) 3D NMC83 electrode structure collected before (primary) and 200 cycles in different electrolytes (E1, E1.5, and E2.5) (dark grey: NMC83 particle, carbon black, and binder; orange: pore). The corner is cut to show the internal morphology. (b) The Pore Network Model is based on the XCT results, and the intensity bar represents the transport distance in the connectivity network. (c) Pore equivalent diameter screening based on the XCT results. (d) Percolation model mechanism.

concentrations (1 M, 2 M, and 2.5 M). Through the application of PNM, high-resolution techniques, and EqD analysis, the ability to alleviate concentration polarization was compared under different electrolyte concentrations, demonstrating that adequate supply of lithium ions and uniform CEI layers are crucial for mitigating concentration polarization and achieving the optimal electrochemical performance of high-loading electrodes. Furthermore, it should be noted that these findings are applicable to other battery materials such as $LiFePO_4$, $LiCoO_2$, and silicon. This study is anticipated to have practical implications in the field of industry, with the goal of mitigating technical challenges associated with high-loading electrodes.

CRediT authorship contribution statement

Ouyang Xiaoping: Funding acquisition, Formal analysis. **Ren Xiangzhong:** Formal analysis. **Yang Xuming:** Formal analysis. **Huang Weiyuan:** Formal analysis. **Pan Feng:** Writing – review & editing, Writing – original draft, Investigation, Conceptualization. **Liu Jianhong:** Funding acquisition, Formal analysis. **Xiao Biwei:** Investigation, Conceptualization. **Chen Weibin:** Writing – review & editing, Writing – original draft, Investigation, Data curation, Conceptualization. **Chen Jing:** Formal analysis. **Wang Kai:** Investigation. **Huang Tao:** Formal analysis. **Hu Jiangtao:** Writing – original draft, Investigation, Funding acquisition, Formal analysis, Conceptualization. **Chen Xi:** Formal analysis. **Zhang Qianling:** Funding acquisition, Conceptualization. **He Xuanlong:** Formal analysis.

Declaration of Competing Interest

The authors declare that they have no known competing financial interests or personal relationships that could have appeared to influence the work reported in this paper.

Acknowledgements

This work has been financially backed by Shenzhen Science and Technology Program (No. KJZD20230923115005009), National Natural Science Foundation (NNSF) of China (No. 52202269), Project of Department of Education of Guangdong Province (No. 2022ZDZX3018) and Xiangjiang Lab (22XJ01007) for providing financial support for this work. We are grateful to the Instrumental Analysis Center of Shenzhen University (Xili Campus) for providing the facilities for our material analyzes.

Appendix A. Supporting information

Supplementary data associated with this article can be found in the online version at doi:10.1016/j.nanoen.2025.110950.

Data Availability

Data will be made available on request.

References

[1] J. Liu, Z. Bao, Y. Cui, E.J. Dufek, J.B. Goodenough, P. Khalifah, Q. Li, B.Y. Liaw, P. Liu, A. Manthiram, Y.S. Meng, V.R. Subramanian, M.F. Toney, V. V. Viswanathan, M.S. Whittingham, J. Xiao, W. Xu, J. Yang, X.-Q. Yang, J.-G. Zhang, Pathways for practical high-energy long-cycling lithium metal batteries, Nat. Energy 4 (2019) 180–186.
[2] M. Ue, K. Sakaushi, K. Uosaki, Basic knowledge in battery research bridging the gap between academia and industry, Mater. Horiz. 7 (2020) 1937–1954.
[3] J. Hu, Y. Jiang, S. Cui, Y. Duan, T. Liu, H. Guo, L. Lin, Y. Lin, J. Zheng, K. Amine, F. Pan, 3D-printed cathodes of LiMn1−xFexPO4 nanocrystals achieve both ultrahigh rate and high capacity for advanced lithium-ion battery, Adv. Energy Mater. 6 (2016) 1600856.
[4] Y. Guo, X. Li, H. Guo, Q. Qin, Z. Wang, J. Wang, G. Yan, Visualization of concentration polarization in thick electrodes, Energy Stor. Mater. 51 (2022) 476–485.
[5] Q. Liu, G. Zhu, R. Li, S. Lou, H. Huo, Y. Ma, J. An, C. Cao, F. Kong, Z. Jiang, M. Lu, Y. Tong, L. Ci, G. Yin, J. Wang, Fast lithium transport kinetics regulated by low energy-barrier LixMnO2 for long-life lithium metal batteries, Energy Stor. Mater. 41 (2021) 1–7.
[6] J. Yang, Y. Li, A. Mijailovic, G. Wang, J. Xiong, K. Mathew, W. Lu, B.W. Sheldon, Q. Wu, Gradient porosity electrodes for fast charging lithium-ion batteries, J. Mater. Chem. A 10 (2022) 12114–12124.
[7] J. Hu, B. Wu, X. Cao, Y. Bi, S. Chae, C. Niu, B. Xiao, J. Tao, J. Zhang, J. Xiao, Evolution of the rate-limiting step: From thin film to thick Ni-rich cathodes, J. Power Sources 454 (2020) 227966.
[8] Y. Liu, Y. Zhu, Y. Cui, Challenges and opportunities towards fast-charging battery materials, Nat. Energy 4 (2019) 540–550.
[9] W. Chen, K. Wang, Y. Li, J. Chen, H. Wang, L. Li, H. Li, X. Ren, X. Ouyang, J. Liu, F. Pan, B. Xiao, Q. Zhang, J. Hu, Minimize the electrode concentration polarization for high-power lithium batteries, Adv. Funct. Mater. (2024) 2410926.
[10] J. Hu, H. Guo, Y. Li, H. Wang, Z. Wang, W. Huang, L. Yang, H. Chen, Y. Lin, F. Pan, Understanding Li-ion thermodynamic and kinetic behaviors in concentrated electrolyte for the development of aqueous lithium-ion batteries, Nano Energy 89 (2021) 106413.
[11] Z. Chen, W. Zhang, J. Liu, M. Zhang, S. Li, F. Pan, Influence of Li Content on the Topological Inhibition of Oxygen Loss in Li-Rich Cathode Materials, Adv. Mater. 36 (2024) 2403307.
[12] J. Wu, Z. Ju, X. Zhang, X. Xu, K.J. Takeuchi, A.C. Marschilok, E.S. Takeuchi, G. Yu, Low-tortuosity thick electrodes with active materials gradient design for enhanced energy storage, ACS Nano 16 (2022) 4805–4812.
[13] X. Zhang, Z. Hui, S. King, L. Wang, Z. Ju, J. Wu, K.J. Takeuchi, A.C. Marschilok, A. C. West, E.S. Takeuchi, G. Yu, Tunable porous electrode architectures for enhanced li-ion storage kinetics in thick electrodes, Nano Lett. 21 (2021) 5896–5904.
[14] J. Hu, Y. Ji, G. Zheng, W. Huang, Y. Lin, L. Yang, F. Pan, Influence of electrolyte structural evolution on battery applications: cationic aggregation from dilute to high concentration, Aggregate 3 (2022) e153.
[15] Q.-S. Liu, H.-W. An, X.-F. Wang, F.-P. Kong, Y.-C. Sun, Y.-X. Gong, S.-F. Lou, Y.-F. Shi, N. Sun, B. Deng, J. Wang, J.-J. Wang, Effective transport network driven by tortuosity gradient enables high-electrochem-active solid-state batteries, Natl. Sci. Rev. 10 (2023) nwac272.
[16] Y. Yu, P. Karayaylali, Y. Katayama, L. Giordano, M. Gauthier, F. Maglia, R. Jung, I. Lund, Y. Shao-Horn, Coupled LiPF6 Decomposition and Carbonate Dehydrogenation Enhanced by Highly Covalent Metal Oxides in High-Energy Li-Ion Batteries, J. Phys. Chem. C. 122 (2018) 27368–27382.
[17] K. Mukai, T. Inoue, Y. Kato, S. Shirai, Superior Low-Temperature Power and Cycle Performances of Na-Ion Battery over Li-Ion Battery, ACS Omega 2 (2017) 864–872.
[18] Y. Yamada, J. Wang, S. Ko, E. Watanabe, A. Yamada, Advances and issues in developing salt-concentrated battery electrolytes, Nat. Energy 4 (2019) 269–280.
[19] B. Koo, H. Lee, S. Hwang, J. Lee, Y.-K. Han, K.H. Ahn, C. Lee, H. Lee, Role of Solvent Isomerism in Mixed Carbonate Electrolytes for Li-Ion Batteries, J. Phys. Chem. C. 127 (2023) 18271–18278.
[20] G. Jiang, F. Li, H. Wang, M. Wu, S. Qi, X. Liu, S. Yang, J. Ma, Perspective on High-Concentration Electrolytes for Lithium Metal Batteries, Small Struct. 2 (2021) 2000122.
[21] Y.X. Yao, X. Chen, N. Yao, J.H. Gao, G. Xu, J.F. Ding, C.L. Song, W.L. Cai, C. Yan, Q. Zhang, Unlocking Charge Transfer Limitations for Extreme Fast Charging of Li-Ion Batteries, Angew. Chem. Int. Ed. 62 (2023) e202214828.
[22] H. Duan, C. Wang, R. Yu, W. Li, J. Fu, X. Yang, X. Lin, M. Zheng, X. Li, S. Deng, X. Hao, R. Li, J. Wang, H. Huang, X. Sun, In Situ Constructed 3D Lithium Anodes for Long-Cycling All-Solid-State Batteries, Adv. Energy Mater. 13 (2023) 2300815.
[23] D. Hubble, D.E. Brown, Y. Zhao, C. Fang, J. Lau, B.D. McCloskey, G. Liu, Liquid electrolyte development for low-temperature lithium-ion batteries, Energy Environ. Sci. 15 (2022) 550–578.
[24] Y.-X. Yao, N. Yao, X.-R. Zhou, Z.-H. Li, X.-Y. Yue, C. Yan, Q. Zhang, Ethylene-Carbonate-Free Electrolytes for Rechargeable Li-Ion Pouch Cells at Sub-Freezing Temperatures, Adv. Mater. 34 (2022) 2206448.
[25] Z. Li, W. Tang, Y. Yang, G. Lai, Z. Lin, H. Xiao, J. Qiu, X. Wei, S. Wu, Z. Lin, Engineering Prelithiation of Polyacrylic Acid Binder: A Universal Strategy to Boost Initial Coulombic Efficiency for High-Areal-Capacity Si-Based Anodes, Adv. Funct. Mater. 32 (2022) 2206615.
[26] Y. Lu, C.-Z. Zhao, J.-Q. Huang, Q. Zhang, The timescale identification decoupling complicated kinetic processes in lithium batteries, Joule 6 (2022) 1172–1198.
[27] S. Sun, C.-Z. Zhao, H. Yuan, Z.-H. Fu, X. Chen, Y. Lu, Y.-F. Li, J.-K. Hu, J. Dong, J.-Q. Huang, M. Ouyang, Q. Zhang, Eliminating interfacial O-involving degradation in Li-rich Mn-based cathodes for all-solid-state lithium batteries, Sci. Adv. 8 (2022) eadd5189.
[28] Z. Li, Y.X. Yao, M. Zheng, S. Sun, Y. Yang, Y. Xiao, L. Xu, C.B. Jin, X.Y. Yue, T. Song, P. Wu, C. Yan, Q. Zhang, Electrolyte Design Enables Rechargeable LiFePO4/Graphite Batteries from −80 °C to 80 °C, Angew. Chem. Int. Ed. e202409409 (2024) 1–11.
[29] X. Zhou, J. Huang, Z. Pan, M. Ouyang, Impedance characterization of lithium-ion batteries aging under high-temperature cycling: Importance of electrolyte-phase diffusion, J. Power Sources 426 (2019) 216–222.
[30] Y. Huang, R. Li, S. Weng, H. Zhang, C. Zhu, D. Lu, C. Sun, X. Huang, T. Deng, L. Fan, L. Chen, X. Wang, X. Fan, Eco-friendly electrolytes via a robust bond design for high-energy Li metal batteries, Energy Environ. Sci. 15 (2022) 4349–4361.
[31] P. Bai, X. Ji, J. Zhang, W. Zhang, S. Hou, H. Su, M. Li, T. Deng, L. Cao, S. Liu, X. He, Y. Xu, C. Wang, Formation of LiF-rich Cathode-Electrolyte Interphase by Electrolyte Reduction, Angew. Chem. Int. Ed. 61 (2022) e202202731.
[32] H. Wan, J. Xu, C. Wang, Designing electrolytes and interphases for high-energy lithium batteries, Nat. Rev. Chem. 8 (2024) 30–44.

[33] M. Aghighi, J. Gostick, Pore network modeling of phase change in PEM fuel cell fibrous cathode, J. Appl. Electrochem 47 (2017) 1323–1338.
[34] Z.A. Khan, P.A.G. Salaberri, T.M.M. Heenan, R. Jervis, P.R. Shearing, D. Brett, A. Elkamel, J.T. Gostick, Probing the Structure-Performance Relationship of Lithium-Ion Battery Cathodes Using Pore-Networks Extracted from Three-Phase Tomograms, J. Electrochem. Soc. 167 (2020) 040528.
[35] A. Torayev, A. Rucci, P.C.M.M. Magusin, A. Demortière, V. De Andrade, C.P. Grey, C. Merlet, A.A. Franco, Stochasticity of Pores Interconnectivity in Li–O2 Batteries and its Impact on the Variations in Electrochemical Performance, J. Phys. Chem. Lett. 9 (2018) 791–797.
[36] M.F. Lagadec, R. Zahn, S. Müller, V. Wood, Topological and network analysis of lithium ion battery components: the importance of pore space connectivity for cell operation, Energy Environ. Sci. 11 (2018) 3194–3200.
[37] H. Xiong, R. Qian, Z. Liu, R. Zhang, G. Sun, B. Guo, F. Du, S. Song, Z.-A. Qiao, S. Dai, A Polymer-Assisted Spinodal Decomposition Strategy toward Interconnected Porous Sodium Super Ionic Conductor-Structured Polyanion-Type Materials and Their Application as a High-Power Sodium-Ion Battery Cathode, Adv. Sci. 8 (2021) 2004943.
[38] C. Jo, J. Hwang, W.-G. Lim, J. Lim, K. Hur, J. Lee, Multiscale Phase Separations for Hierarchically Ordered Macro/Mesostructured Metal Oxides, Adv. Mater. 30 (2018) 1703829.
[39] Y. Luo, Y. Bai, A. Mistry, Y. Zhang, D. Zhao, S. Sarkar, J.V. Handy, S. Rezaei, A. C. Chuang, L. Carrillo, K. Wiaderek, M. Pharr, K. Xie, P.P. Mukherjee, B.-X. Xu, S. Banerjee, Effect of crystallite geometries on electrochemical performance of porous intercalation electrodes by multiscale operando investigation, Nat. Mater. 21 (2022) 217–227.
[40] A. Mistry, V. Srinivasan, H.G. Steinrück, Characterizing Ion Transport in Electrolytes via Concentration and Velocity Profiles, Adv. Energy Mater. 13 (2023) 2203690.
[41] A. Shodiev, F.M. Zanotto, J. Yu, M. Chouchane, J. Li, A.A. Franco, Designing electrode architectures to facilitate electrolyte infiltration for lithium-ion batteries, Energy Stor. Mater. 49 (2022) 268–277.
[42] V. Srinivasan, J. Newman, Discharge Model for the Lithium Iron-Phosphate Electrode, J. Electrochem. Soc. 151 (2004) A1517–A1529.
[43] Z. Du, D.L. Wood, C. Daniel, S. Kalnaus, J. Li, Understanding limiting factors in thick electrode performance as applied to high energy density Li-ion batteries, J. Appl. Electrochem 47 (2017) 405–415.
[44] L.S. Kremer, T. Danner, S. Hein, A. Hoffmann, B. Prifling, V. Schmidt, A. Latz, M. Wohlfahrt-Mehrens, Influence of the Electrolyte Salt Concentration on the Rate Capability of Ultra-Thick NCM 622 Electrodes, Batt. Supercaps 3 (2020) 1172–1182.